Gradient Tandem Mass Spectrometry Interfaced with Ion Mobility Separation for the Characterization of Supramolecular Architectures

ARTICLE *in* ANALYTICAL CHEMISTRY · FEBRUARY 2011

Impact Factor: 5.64 · DOI: 10.1021/ac1022875 · Source: PubMed

4 AUTHORS, INCLUDING:

Xiaopeng Li
University of Akron
45 PUBLICATIONS **1,043** CITATIONS
SEE PROFILE

George Richard Newkome
University of Akron
500 PUBLICATIONS **13,013** CITATIONS
SEE PROFILE

Chrys Wesdemiotis
University of Akron
260 PUBLICATIONS **5,722** CITATIONS
SEE PROFILE

analytical chemistry

ARTICLE

pubs.acs.org/ac

Gradient Tandem Mass Spectrometry Interfaced with Ion Mobility Separation for the Characterization of Supramolecular Architectures

Xiaopeng Li,[†] Yi-Tsu Chan,[‡] George R. Newkome,*[,†,‡] and Chrys Wesdemiotis*[,†,‡]

[†]Departments of Chemistry and [‡]Polymer Science, The University of Akron, Akron, Ohio 44325, United States

Supporting Information

ABSTRACT: Traveling wave ion mobility mass spectrometry (TWIM MS) was combined with gradient tandem mass spectrometry (gMS^2) to deconvolute and characterize superimposed ions with different charges and shapes formed by electrospray ionization (ESI) of self-assembled, hexameric metallomacrocycles composed of terpyridine-based ligands and Cd^{II} ions. ESI conditions were optimized to obtain intact hexameric cation assemblies in a low charge state (2+), in order to minimize overlapping fragments of the same mass-to-charge ratio. With TWIM MS, intact hexameric ions could be separated from remaining fragments and aggregates. Collisional activation of these hexameric ions at varying collision energies (gMS^2), followed by TWIM separation, was then performed to resolve macrocyclic from linear hexameric species. Because of the different stabilities of these architectures, gMS^2 changes their relative amounts, which can be monitored individually after subsequent ion mobility separation. On the basis of this unique strategy, hexameric cyclic and linear isomers have been successfully resolved and identified. Complementary structural information was gained by the gMS^2 fragmentation pattern of the metallosupramolecules, acquired by collisionally activated dissociation after TWIM dispersion. TWIM MS interfaced with gMS^2 should be particularly valuable for the characterization of a variety of supramolecular polymers, which often contain isomeric architectures that yield overlapping fragments and aggregates upon ESI MS analysis.

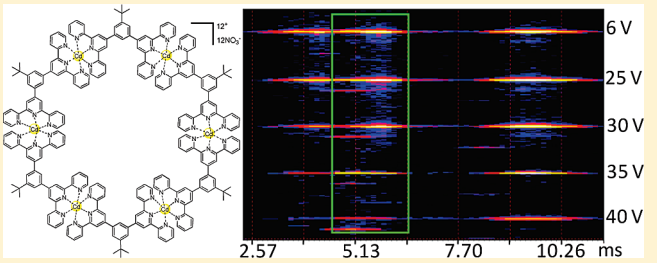

Coordination interactions are widely employed in the self-assembly of supramolecular structures.[1−7] X-ray crystallography and NMR spectroscopy, which provide both stoichiometry and shape information, have generally been used to characterize such supramolecules. Because of the difficulty of obtaining single crystals suitable for X-ray diffraction and sensitivity and/or stereogenic problems in NMR experiments,[8−10] electrospray ionization mass spectrometry (ESI MS) has become increasingly important for the detection of supramolecular constructs and the analysis of their compositions.[11−15] Obstacles do exist, however, in ESI MS characterizations. If the noncovalent binding interactions in a supramolecule are weak, ESI can cause fragmentation. With metal-bound supramolecular assemblies composed of identical subunits, the fragments often have the same mass-to-charge (m/z) ratios as the intact assemblies and, thus, their isotope clusters overlap. Further, several of the counterions used to balance the metal charges undergo eliminations during ESI; for example, BF_4^- and PF_6^-, two very common anions in organometallic self-assemblies, can lose BF_3 and PF_5, respectively, which complicates the ESI mass spectra. Moreover, the transition metals typically used in self-assembly processes contain many isotopes, leading to broad signals for each composition and charge state. These obstacles can be partly overcome with cold-spray ionization (CSI), which improves the intensity of intact supramolecular ions by reducing the internal energy deposited in the ionization step.[11,14,16,17] On the other hand, Fourier transform ion cyclotron resonance (FTICR) mass spectrometry, which exhibits exceptional resolving power, may be used to deconvolute the isotope patterns of isobaric charge states arising from the intact supramolecular ions and their fragments.[12,18,19] Unfortunately, CSI sources using liquid nitrogen require sophisticated, custom-made instrumentation (available in one laboratory only) and easily produce solvent adducts.[14,16,17] Conversely, FTICR MS cannot deconvolute the isotope patterns of the intact supramolecular ion from those of superimposed fragments with exactly the same m/z values, a situation encountered with highly symmetrical structures, self-assembled from a large number of identical repeating units;[12,18,19] and neither CSI nor FTICR MS can separate isomeric architectures. These problems make it obvious that alternative analytical methods are necessary to characterize properly supramolecular polymers.

A means to address and resolve the described limitations is provided by ion mobility mass spectrometry (IM MS), which in the past decade has advanced into a powerful method for the separation of isobars, isomers, and conformers from many different types of analytes.[20−34] IM MS may be viewed as a gas-phase ion chromatography method, in which ions drift against a gas stream under the influence of an electric field. The drift time

Received: August 30, 2010
Accepted: January 3, 2011
Published: January 24, 2011

Scheme 1. Hexacadmium Macrocycles 1 and 2, Carrying Methyl and *tert*-Butyl Groups, Respectively, In Their Terpyridine-Based Ligands[a]

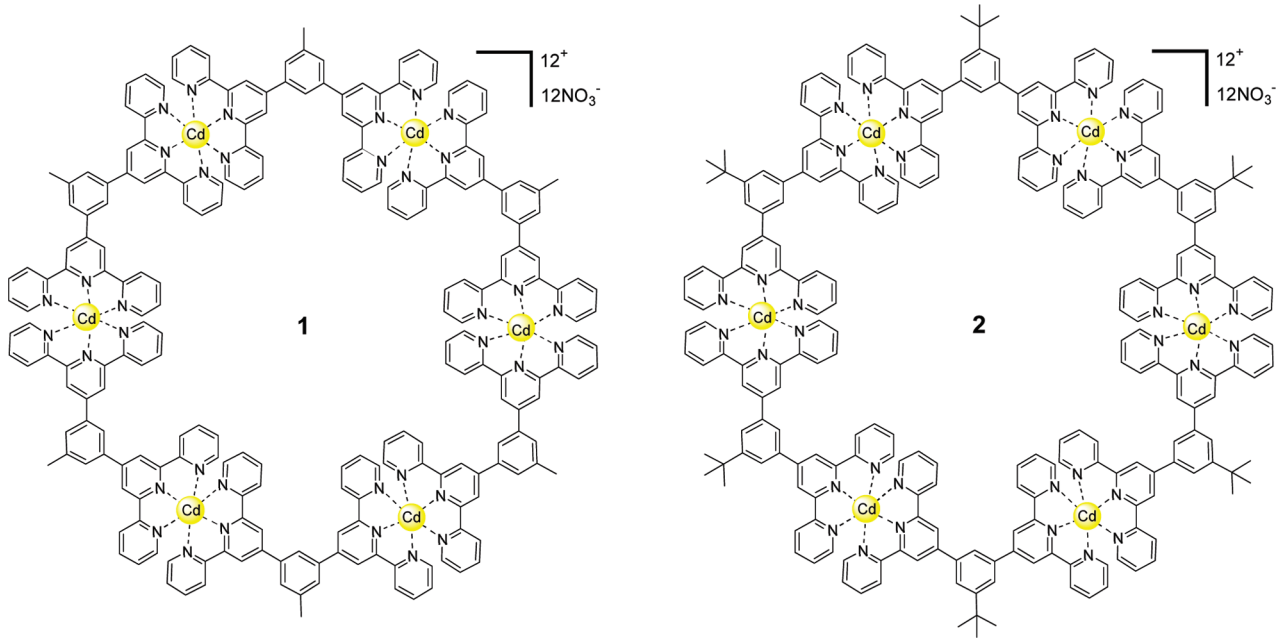

[a] The six Cd^{II} ions provide 12+ charges which are balanced by 12 NO_3^- anions.

of an ion through the IM region (drift region) depends on the ion's mass, charge, and shape. Hence, isomeric (or isobaric ions) can be dispersed according to their charge states and architectures. Inspired by this capability, we recently applied for the first time a variant of IM MS, viz., traveling wave ion mobility mass spectrometry (TWIM MS),[35−50] to supramolecular assemblies,[51−53] including coordinatively bound metallomacrocycles[51,53] and $\pi-\pi$ bonded polymers.[52] With TWIM MS, it was possible to separate intact supramolecular species from fragments with an identical m/z ratio as well as different supramolecular isomers with the same charge. Similar results have been reported by Bowers and co-workers in a later IM MS study of rigid triangular and rectangular organometallic assemblies.[54] In the present study, hexameric metallomacrocycles **1** and **2** (Scheme 1) are used to determine the optimal experimental conditions for forming intact macromolecular ions in low charge states and large m/z ratios, so that the content of superimposed isobaric fragments is minimized. The isomeric composition of the intact supramolecular species is subsequently characterized by gradient tandem mass spectrometry (referred to as gradient MS^2 or gMS^2); this involves collisionally activated dissociation (CAD) at different collision energies, combined with TWIM separation of either the precursor ion components (TWIM precedes CAD) or their fragments (TWIM follows CAD). Gradient MS^2 deconvolutes the architectures present in the selected m/z ratio and identifies them based on the energy dependence of their fragmentation and resulting fragmentation patterns.

EXPERIMENTAL SECTION

The electrospray ionization traveling wave ion mobility mass spectrometry (ESI TWIM MS) experiments were performed with a Waters Synapt quadrupole/time-of-flight (Q/TOF) mass spectrometer (Waters Corp., Milford, MA). The ESI source and desolvation temperatures were set at 30 and 40 °C, respectively, and the desolvation gas (N_2) flow was adjusted at 800 L/h. The sample solutions were introduced into the source region of the instrument by direct infusion at a flow rate of 10 μL/min. For the acquisition of ESI mass spectra, the ESI capillary and sample cone voltages were optimized within the 2−3 kV and 15−64 V ranges, respectively, while the extraction cone voltage was set at 3.2 V. The Synapt Q/TOF mass spectrometer contains a traveling wave ion mobility device between the Q and TOF mass analyzers, consisting of three collision cells arranged in the order trap cell, ion mobility cell, and transfer cell. Trap and transfer cells are pressurized with Ar (1.5 mL/min flow rate), and the ion mobility cell with N_2 (22.7 mL/min flow rate). In MS mode, potentials of 6 and 4 V were applied to the trap and collision cells, respectively, and Q was set in rf-only mode to transmit all ions exiting the ESI source. In MS^2 experiments, Q was adjusted to transmit only ions of a selected m/z ratio. For CAD before ion mobility separation, the trap cell potential was varied within 6−60 V to induce fragmentation at different collision energies; conversely, CAD after ion mobility separation was effected by raising the transfer cell potential within 4−60 V. All ion mobility separations were performed at a traveling wave velocity of 350 m/s and a traveling wave height of 13 V. The ions exiting the transfer cell were accelerated orthogonally into the TOF analyzer for mass analysis. The total acquisition time for each MS and MS^2 spectrum shown was 5 min. Data acquisition and processing were conducted using the MassLynx (v 4.1) and drift scope (v 2.1) programs of Waters Corp. The hexacadmium macrocycles **1** and **2** were synthesized according to previously published procedures.[51] The sprayed solutions were prepared by dissolving 1 mg of sample in 1 mL of 3:2 (v/v) $CHCl_3$/MeOH solvent mixture. HPLC-grade solvents were purchased from Fisher Scientific (Pittsburgh, PA) and were used in the condition received without further purification.

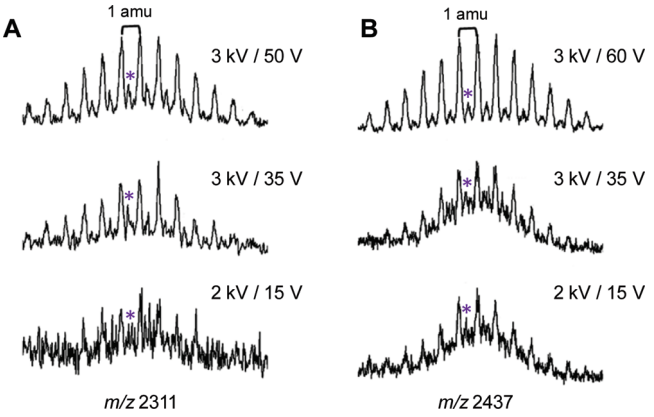

Figure 1. Effect of ESI capillary and sample cone voltages on the intensity and isotope resolution of hexameric $[6L + 6Cd]^{2+}$ ions from (A) **1** (m/z 2311) and (B) **2** (m/z 2437). The asterisk denotes a peak of the $[6L + 6Cd]^{2+}$ isotope cluster.

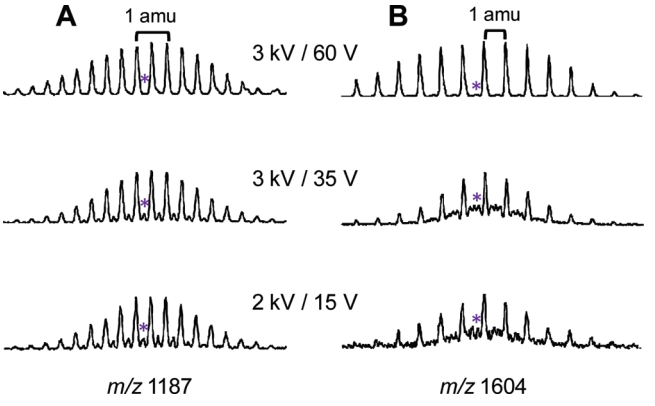

Figure 2. Effect of ESI capillary and sample cone voltages on the intensity and isotope resolution of hexameric ions from **2** in high charge states; (A) $[6L + 6Cd]^{4+}$ (m/z 1187) and (B) $[6L + 6Cd]^{3+}$ (m/z 1604). The asterisk denotes a peak of the $[6L + 6Cd]^{4+}$ or $[6L + 6Cd]^{3+}$ isotope clusters (which essentially disappear at the highest voltage settings).

RESULTS AND DISCUSSION

Because of the labile nature of the ⟨tpy−Cd^{II}−tpy⟩ connectivity, the ESI source and desolvation temperatures must be kept low and the desolvation gas flow high in order to maximize the ion intensities produced from hexameric metallomacrocycles **1** and **2** (see the Experimental Section for the actual settings). With the low ESI capillary and sample cone voltages typically used for supramolecular analytes (2.5 kV and 35 V, respectively),[51,52] high charge states of **1** and **2** dominate.[51] In our initial TWIM MS investigation of **1** and **2**, triply and quadruply charged precursor ions were therefore selected for ion mobility separation.[51] Highly charged hexameric ions may overlap with several lower charge state fragments and higher charge state aggregates. For example, m/z 1604 from complex **2** was shown to contain $[2L + 2Cd]^{1+}$ and $[4L + 4Cd]^{2+}$ fragments (L = tpy ligand), intact hexameric $[6L + 6Cd]^{3+}$ ions, as well as $[8L + 8Cd]^{4+}$ clusters generated via aggregation of the smaller fragments (these ions also contain 3, 6, 9, and 12 NO_3^- counterions, respectively, which have been omitted for brevity). The drift time of intact $[6L + 6Cd]^{3+}$ through the TWIM cell fell between those of $[4L + 4Cd]^{2+}$ and $[8L + 8Cd]^{4+}$, and the corresponding drift time distributions were partly superimposed, making it impossible to separate the cyclic and linear architectures of $[6L + 6Cd]^{3+}$. This goal could be achieved for m/z 1187 (from **2**) due to the fortuitously low number of L/Cd combinations at this mass-to-charge ratio (with the tpy ligand of **2**), which permitted the separation and detection of a minor linear $[6L + 6Cd]^{4+}$ component next to the major macrocyclic $[6L + 6Cd]^{4+}$ structure.[51] The isotope resolution of the more highly charged ion was, however, poorer.

A lesser overlap with fragments and a better isotope resolution should be obtainable with lower charge states, as these contain fewer isotopes within one m/z unit and appear at m/z ratios that are larger than those of most fragments; this premise was examined for **1** and **2**. For improved sensitivity, the samples were precooled overnight at −8 °C, as described in the literature.[11] The parameters that were found to influence most dramatically isotope resolution and the relative abundances of the various charge states are the voltages applied to the ESI capillary and sample cone. At the low voltages commonly used to minimize in-source fragmentation,[15] doubly charged **1** (m/z 2311) and **2** (m/z 2437) are minuscule and their isotopes poorly resolved, cf. Figure 1, bottom; as mentioned above these settings maximize more highly charged species. A gradual improvement in both isotope resolution and sensitivity is observed as the ESI capillary and sample cone voltages are raised (Figure 1, center). Signal intensity and isotope resolution of the 2+ state, i.e., $[6L + 6Cd]^{2+}$, maximize at 3 kV/50−60 V (Figure 1, top), which were the values chosen for the TWIM MS experiments (*vide infra*); further increases start depleting $[6L + 6Cd]^{2+}$ by promoting extensive dissociation to $[3L + 3Cd]^{1+}$ and smaller fragments. Note that the higher voltage settings optimizing the $[6L + 6Cd]^{2+}$ signal intensity substantially reduce the intensities of the higher charge states (3+ and 4+), which dissociate more readily due to increased repulsion between the like charges, cf. Figure 2 (see the Supporting Information for the full ESI mass spectrum of **2**). Superimposed highly charged aggregates may also dissociate under these conditions to yield hexameric $[6L + 6Cd]^{2+}$ ions of macrocyclic or linear structure; the repercussions of this process will be discussed later.

Figure 3 shows the drift time distributions arising after ion mobility separation of m/z 2311 (from **1**) and 2437 (from **2**). Several signals are detected at each m/z ratio. On the basis of the corresponding isotope patterns, doubly charged $[6L + 6Cd]^{2+}$ and singly charged $[3L + 3Cd]^{1+}$ are observed from both **1** (at 4.87 and 8.34 ms, respectively) as well as **2** (at 5.64 and 9.36 ms, respectively). Additionally, both samples show clusters in higher charge states (>2+), which probably originate from aggregation of smaller singly and/or doubly charged ions with combined m/z values of 2311 (from **1**) or 2437 (from **2**); such aggregates are common at the sample cone voltage and desolvation temperature employed in this study.[15,51] Since only one peak is observed for the hexameric $[6L + 6Cd]^{2+}$ ions from **1** and **2**, it is difficult to determine the corresponding architectures (cyclic vs linear) from the drift time distributions alone. The $[6L + 6Cd]^{2+}$ signals are broad, and (especially) the one from **2** clearly shows a shoulder on its left side, pointing out that more than one $[6L + 6Cd]^{2+}$ isomer may be present. Two different approaches have been utilized in previous studies to identify the structures probed in TWIM MS experiments. The drift times observed can be converted to collision cross sections[54−56] for comparison with the cross sections predicted for individual (e.g., macrocyclic vs linear) architectures by molecular modeling.[21−23,26,54,57,58] Alternatively, reference compounds of established structure may

be used to elucidate the unknown structure(s) based on the corresponding TWIM MS characteristics.[51] Here, we introduce a new experimental procedure, involving gradient tandem mass spectrometry, to deconvolute ill-resolved isomers and characterize their architectures.

With the Synapt Q/TOF mass spectrometer, MS^2 experiments via CAD can be conducted either before ion mobility separation in the trap cell or after ion mobility separation in the transfer cell. CAD of the hexameric $[6L + 6Cd]^{2+}$ ions mainly yields $[3L + 3Cd]^{1+}$ fragments, which have the same m/z ratio as the precursor ions. If MS^2 is performed in the transfer cell, i.e., after ion mobility separation, the $[3L + 3Cd]^{1+}$ fragments would be superimposed with the $[6L + 6Cd]^{2+}$ precursor ions. Hence, the fragmentation behavior of $[6L + 6Cd]^{2+}$ was probed in the trap, followed by separation of the precursor and fragment ions by the ion mobility device.

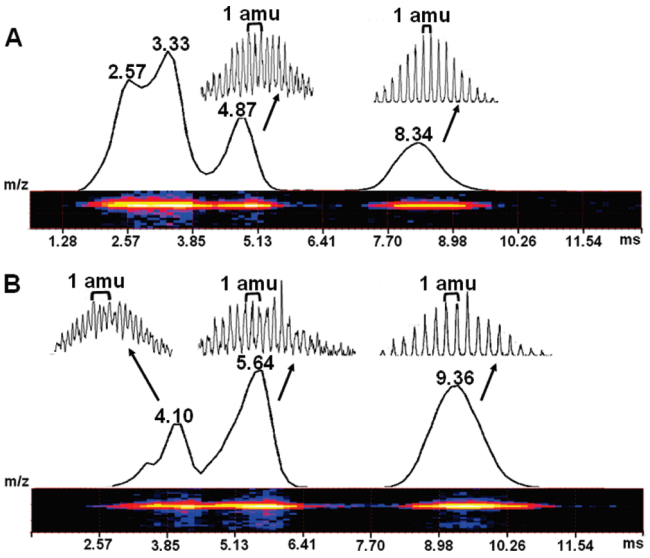

Figure 3. Two-dimensional ESI TWIM MS plots for (A) m/z 2311 from **1** and (B) m/z 2437 from **2**. Ion mobility separation was effected using a traveling wave height of 13 V and a traveling wave velocity of 350 m/s. (A) The precursor ion from **1** gives rise to signals at 2.57, 3.33, 4.87, and 8.34 ms; on the basis of the isotope patterns observed, the signals at 4.87 and 8.34 ms correspond to $[6L + 6Cd]^{2+}$ and $[3L + 3Cd]^{1+}$, respectively, and those at 2.57 and 3.33 ms to higher charge state (>2+) clusters. (B) The precursor ion from **2** gives rise to signals at 4.10, 5.64, and 9.36 ms; their isotope patterns agree well with $[9L + 9Cd]^{3+}$, $[6L + 6Cd]^{2+}$, and $[3L + 3Cd]^{1+}$, respectively. The shoulder at low drift time most likely originates from >3+ clusters.

Figure 4 shows the components of m/z 2311 from **1**, monitored after CAD and TWIM separation, as a function of collision energy. When the voltage applied to the trap cell is increased from 6 to 25 V, the left shoulder of the signal at 4.87 ms becomes a resolved peak with a maximum at 4.10 ms. At 30 V, two almost equally abundant signals are observed at 4.10 and 4.87 ms, both representing hexameric $[6L + 6Cd]^{2+}$ ions according to the corresponding isotope patterns. It has been well documented that compact ions drift faster than isomers with more extended structures upon ion mobility separation.[20−33,38−54,57,58] The organometallic assemblies studied here can exist in cyclic as well as linear architectures; with tpy ligands having a 120°-geometry between the metal binding sites (as those in **1** and **2**) macrocyclic structures are favored, whereas ligands with a 180°-arrangement of their binding sites form exclusively linear structures.[51] On the basis of these facts, the signals at 4.10 and 4.87 ms are assigned to cyclic $[6L + 6Cd]^{2+}$ and linear $[6L + 6Cd]^{2+}$, respectively. If the voltage of the trap cell is increased further to 35−40 V, cyclic $[6L + 6Cd]^{2+}$ becomes the major hexameric component of m/z 2311, while at the lowest collision energy (6 eV), linear $[6L + 6Cd]^{2+}$ was the major hexameric component. The gradual change in relative amounts of linear and cyclic $[6L + 6Cd]^{2+}$ reflects the corresponding isomer stabilities. The cyclic $[6L + 6Cd]^{2+}$ ions require cleavage of more bonds for fragmentation and, thus, can survive undissociated at higher internal energies than the linear isomers.[51,53] This stability difference is exploited in gradient MS^2 to distinguish and identify isomers that are not well resolved under nonactivating conditions. At voltages ≥40 V, the absolute intensity of $[3L + 3Cd]^{1+}$ also decreases (see 2-D trace in Figure 4, right) due to consecutive dissociation to smaller fragments.

The gradient MS^2 strategy was also applied to m/z 2437 from **2** to separate cyclic and linear isomers. As before, cyclic and linear $[6L + 6Cd]^{2+}$ are effectively separated at an elevated trap cell voltage (35 V in this case), giving rise to distinct drift time distributions with maxima at 4.87 and 5.64 ms, respectively (cf. Figure 5). Again, the cyclic ions increase in abundance, relative to the linear species, at the higher collision energies, consistent with

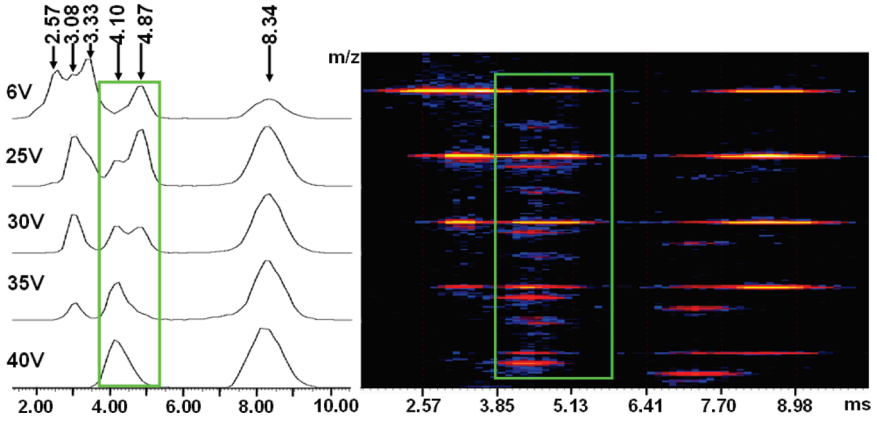

Figure 4. Two-dimensional ESI MS^2 TWIM plot of m/z 2311 from **1**. CAD took place in the trap cell (before ion mobility separation) at different collision energies, varied by raising the potential applied to the trap from 6 to 40 V. The ions exiting the trap were subsequently separated in the ion mobility region. $[6L + 6Cd]^{2+}$ species are encased in a green-highlighted rectangle.

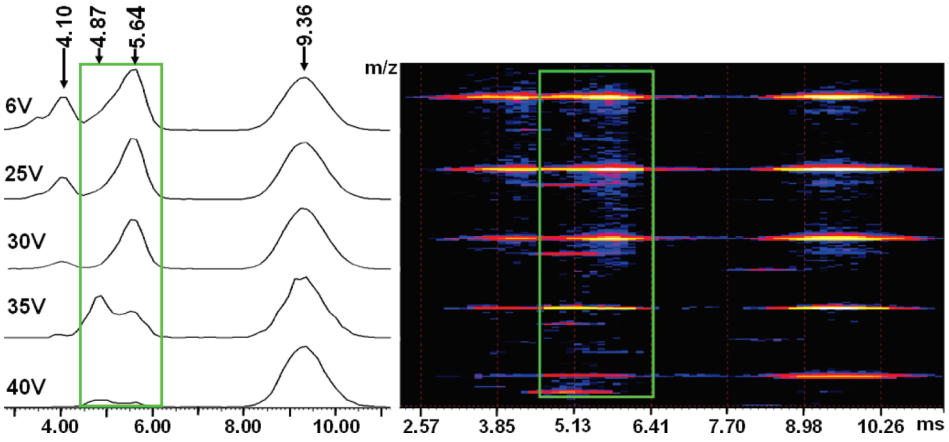

Figure 5. Two-dimensional ESI MS^2 TWIM plot of m/z 2327 from **2**. CAD took place in the trap cell (before ion mobility separation) at different collision energies, varied by raising the potential applied to the trap from 6 to 40 V. The ions exiting the trap were subsequently separated in the ion mobility region. $[6L + 6Cd]^{2+}$ species are encased in a green-highlighted rectangle.

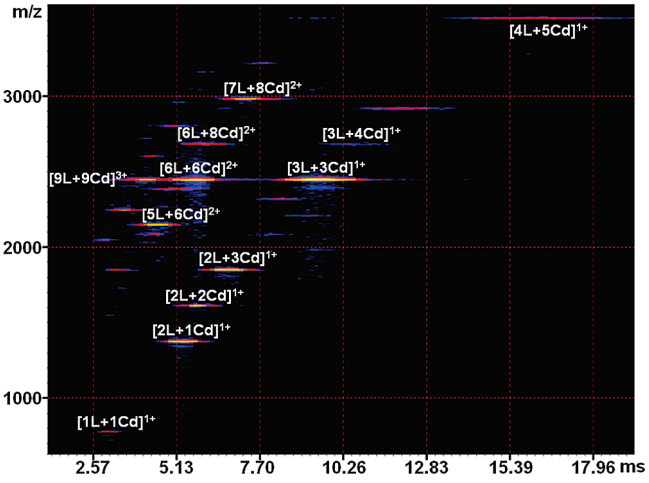

Figure 6. 2-D ESI MS^2 TWIM plot showing the fragments of m/z 2437 (from **2**) generated by CAD in the trap cell (at a collision energy of 30 eV) followed by ion mobility separation.

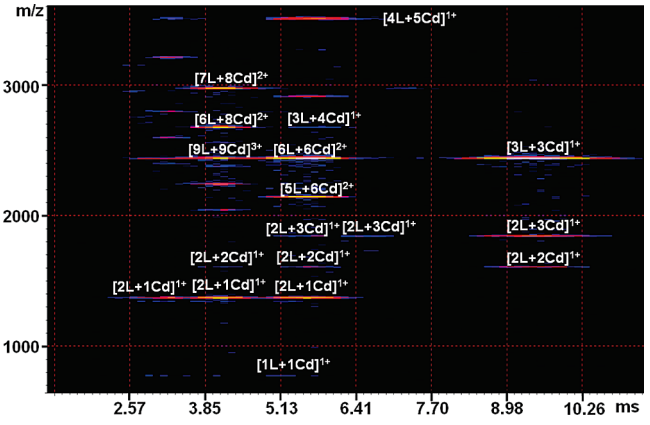

Figure 7. 2-D ESI TWIM MS^2 plot showing the fragments of m/z 2437 (from **2**) generated after ion mobility separation of the components of m/z 2437 followed by CAD in the transfer cell (at a collision energy of 35 eV).

their higher stability. At trap cell voltages ≥40 V, consecutive dissociations become significant, depleting the intensities of both $[6L + 6Cd]^{2+}$ and $[3L + 3Cd]^{1+}$.

It is worth noting that the highly charged (>2+) clusters at m/z 2311 or 2437 also dissociate during the MS^2 experiment. Because of their weak bonding, these clusters may already fragment at the lowest activation conditions. Their dissociation products most likely include cyclic and linear $[6L + 6Cd]^{2+}$ (*vide infra*), which are observed together with the cyclic and linear $[6L + 6Cd]^{2+}$ ions arriving from the ESI source. Such contribution to $[6L + 6Cd]^{2+}$ from cluster dissociation reconciles the high relative abundance of the linear $[6L + 6Cd]^{2+}$ at 6 V. TWIM MS experiments on the 4+ charge state of hexameric **2**, which contains no superimposed cluster ions, showed that the major hexameric complex structure formed in the synthesis (>95%) is the macrocycle.[51]

The complete MS^2 fragmentation pattern of the hexameric $[6L + 6Cd]^{2+}$ ions has also been assessed at varying collision energies. The precursor ions at m/z 2311 (from **1**) and m/z 2437 (from **2**) yield very similar spectra; those from **2**, acquired via CAD in the trap cell at 30 eV collision energy or the transfer cell at 35 eV, are shown in Figures 6 and 7, respectively, in the form of 2-D plots of m/z vs drift time. The majority of fragments detected in the MS^2 TWIM spectrum (CAD in the trap cell, Figure 6) contain <6 tpy ligands and ≤6 Cd^{II} ions, consistent with generation from a $[6L + 6Cd]^{2+}$ precursor ion. There are, however, a few larger fragments, viz., $[6L + 8Cd]^{2+}$ and $[7L + 8Cd]^{2+}$, which could originate from dissociation of the cluster ions in high charge states (e.g., $[9L + 9Cd]^{3+}$) or through ion−molecule reactions of $[6L + 6Cd]^{2+}$ in the trap and/or ion mobility cell. This question is answered by looking at the TWIM MS^2 spectrum (CAD in the transfer cell, Figure 7). The products generated at this location are formed after ion mobility separation and have the same drift times as their precursors. It is evident from Figure 7 that hexameric $[6L + 6Cd]^{2+}$ yields only fragments with <6 tpy ligands and ≤6 Cd^{II} ions (note that the $[3L + 3Cd]^{1+}$ fragment generated from $[6L + 6Cd]^{2+}$ overlaps with the precursor ion in this case). The fragments with >6 tpy ligands or Cd^{II} ions, viz., $[6L + 8Cd]^{2+}$ and $[7L + 8Cd]^{2+}$, are produced exclusively from $[9L + 9Cd]^{3+}$; hence, associative ion molecule reactions do not take place in the gMS^2 (or MS^2) experiments. It is noteworthy that CAD of $[6L + 6Cd]^{2+}$ yields fragments with 1−5 tpy ligands and 1−6 Cd^{II} ions (Figure 7),

pointing out that fragmentation can occur at any of the coordinative bonds of **2**. In contrast, $[9L + 9Cd]^{3+}$ gives rise to fewer fragments, as expected from a cluster (or mixture of clusters), which should primarily decompose into its (their) components.

The MS^2 fragmentation patterns of metallomacrocyclic ions and their linear isomers are indistinguishable. This was demonstrated in an earlier study by comparison of the dissociation products of $[6L + 6Cd]^{4+}$ from **2** with those of an isomeric hexamer carrying tpy ligands with a 180°-geometry of their metal binding sites, with which only linear complexes are possible.[51] The sole difference in the corresponding CAD spectra was in the relative abundances of the $[6L + 6Cd]^{4+}$ precursor ions, with the cyclic structure showing intact, undissociated $[6L + 6Cd]^{4+}$ species in much higher intensity (under identical activation conditions);[51] the same trend is observed in our gMS^2 experiments described here (Figures 4 and 5). The lower dissociation extent of the macrocyclic structure results from a higher thermodynamic stability, imparted by the better coordination of all metal ions in the macrocycle, and the higher kinetic stability resulting from having to break more bonds in a cyclic than a linear complex, in order to form the same fragments.

CONCLUSIONS

ESI MS has been optimized to obtain intact macromolecular ions of low charge state and high m/z ratio from self-assembled hexagonal metallomacrocycles with the labile ⟨tpy−Cd^{II}−tpy⟩ connectivity. TWIM MS can separate the intact macrocyclic ions from overlapping fragments and aggregates. Further resolution of the hexagonal macrocyclic structures from coexisting linear isomers can be achieved by gradient MS^2 experiments performed in the trap cell (CAD before TWIM separation). In gMS^2, the energy available for fragmentation is gradually increased, which affects the relative intensities of isomers with different stabilities. Coordinatively bound macrocyclic and linear isomers are readily deconvoluted because of the lower stabilities of the latter constructs. Additional structural information is obtained from MS^2 spectra acquired using the transfer cell (CAD after ion mobility separation); these unveil the complete fragmentation pattern of the metallosupramolecule, which is diagnostic for the corresponding connectivity. Overall, ESI TWIM MS and gradient MS^2 provide an ideally suitable method for the characterization of supramolecular architectures.

ASSOCIATED CONTENT

Supporting Information. Additional information as noted in text. This material is available free of charge via the Internet at http://pubs.acs.org.

AUTHOR INFORMATION

Corresponding Author

*Fax: (330) 972-6085. E-mail: wesdemiotis@uakron.edu (C.W.); newkome@uakron.edu (G.R.N.).

ACKNOWLEDGMENT

We thank the National Science Foundation for generous financial support (Grants CHE-0517909 and 1012636 to C.W., Grant DMR-0705015 to G.R.N., and Grant DMR-0821313 for the purchase of the instrument for the TWIM MS studies).

REFERENCES

(1) Holliday, B. J.; Mirkin, C. A. *Angew. Chem., Int. Ed.* **2001**, *40*, 2022–2043.
(2) Ruben, M.; Rojo, J.; Romero-Salguero, F. J.; Uppadine, L. H.; Lehn, J.-M. *Angew. Chem., Int. Ed.* **2004**, *43*, 3644–3662.
(3) Fujita, M.; Tominaga, M.; Hori, A.; Therrien, B. *Acc. Chem. Res.* **2005**, *38*, 371–380.
(4) Constable, E. C. *Coord. Chem. Rev.* **2008**, *252*, 842–855.
(5) Kumar, A.; Sun, S. S.; Lees, A. J. *Coord. Chem. Rev.* **2008**, *252*, 922–939.
(6) Lee, S. J.; Lin, W. *Acc. Chem. Res.* **2008**, *41*, 521–537.
(7) Li, S. S.; Northrop, B. H.; Yuan, Q. H.; Wan, L. J.; Stang, P. J. *Acc. Chem. Res.* **2009**, *42*, 249–259.
(8) Moucheron, C.; Kirsch-De Mesmaeker, A.; Dupont-Gervais, A.; Leize, E.; Van Dorsselaer, A. *J. Am. Chem. Soc.* **1996**, *118*, 12834–12835.
(9) Kriesel, J. W.; König, S.; Freitas, M. A.; Marshall, A. G.; Leary, J. A.; Tilley, T. D. *J. Am. Chem. Soc.* **1998**, *120*, 12207–12215.
(10) Newkome, G. R.; Cho, T. J.; Moorefield, C. N.; Baker, G. R.; Cush, R.; Russo, P. S. *Angew. Chem., Int. Ed.* **1999**, *38*, 3717–3721.
(11) Wang, P.; Newkome, G. R.; Wesdemiotis, C. *Int. J. Mass Spectrom.* **2006**, *255−256*, 86–92.
(12) Engeser, M.; Rang, A.; Ferrer, M.; Gutierrez, A.; Baytekin, H. T.; Schalley, C. A. *Int. J. Mass Spectrom.* **2006**, *255−256*, 185–194.
(13) Zheng, Y. R.; Stang, P. J. *J. Am. Chem. Soc.* **2009**, *131*, 3487–3489.
(14) Sato, S.; Ishido, Y.; Fujita, M. *J. Am. Chem. Soc.* **2009**, *131*, 6064–6065.
(15) Lusby, P. J.; Müller, P.; Pike, S. J.; Slawin, A. M. Z. *J. Am. Chem. Soc.* **2009**, *131*, 16398–16400.
(16) Sakamoto, S.; Fujita, M.; Yamaguchi, K. *Tetrahedron* **2000**, *56*, 955–964.
(17) Yamaguchi, K. *J. Mass Spectrom.* **2003**, *38*, 473–490.
(18) Schalley, C. A.; Müller, T.; Linnartz, P.; Witt, M.; Schäfer, M.; Lützen, A. *Chem.—Eur. J.* **2002**, *8*, 3538–2551.
(19) Jiang, W.; Schäfer, M.; Mohr, P. C.; Schalley, C. A. *J. Am. Chem. Soc.* **2010**, *132*, 2309–2320.
(20) Von Helden, G.; Hsu, M.-T.; Kemper, P. R.; Bowers, M. T. *J. Chem. Phys.* **1991**, *95*, 3835–3837.
(21) Bowers, M. T.; Kemper, P. R.; von Helden, G.; Koppen, P. A. M. *Science* **1993**, *260*, 1446–1451.
(22) Clemmer, D. E.; Jarrold, M. F. *J. Mass Spectrom.* **1997**, *32*, 577–592.
(23) Hoaglund-Hyzer, C. S.; Counterman, A. E.; Clemmer, D. E. *Chem. Rev.* **1999**, *99*, 3037–3080.
(24) Verbeck, G. F.; Ruotolo, B. T.; Sawyer, A. A.; Gillig, K. J.; Russell, D. H. *J. Biomol. Techn.* **2002**, *13*, 56–61.
(25) Valentine, S. J.; Plasencia, M. D.; Liu, X.; Krishnan, M.; Naylor, S.; Udseth, H. R.; Smith, R. D.; Clemmer, D. E. *J. Proteome Res.* **2006**, *5*, 2977–2984.
(26) Trimpin, S.; Plasencia, M.; Isailovic, D.; Clemmer, D. E. *Anal. Chem.* **2007**, *79*, 7965–7974.
(27) Bohrer, B. C.; Merenbloom, S. I.; Koeniger, S. L.; Hilderbrand, A. E.; Clemmer, D. E. *Annu. Rev. Anal. Chem.* **2008**, *1*, 293–327.
(28) Trimpin, S.; Clemmer, D. E. *Anal. Chem.* **2008**, *80*, 9073–9083.
(29) Anderson, S. E.; Bodzin, D. J.; Haddad, T. S.; Boatz, J. A.; Mabry, J. M.; Mitchell, C.; Bowers, M. T. *Chem. Mater.* **2008**, *20*, 4299–4309.
(30) Fenn, L. S.; McLean, J. A. *Anal. Bioanal. Chem.* **2008**, *391*, 905–909.
(31) Kanu, A. B.; Dwivedi, P.; Tam, M.; Matz, L.; Hill, H. H. *J. Mass Spectrom.* **2008**, *43*, 1–22.
(32) Ruotolo, B. T.; Benesch, J. L. P.; Sandercock, A. M.; Hyung, S. J.; Robinson, C. V. *Nat. Protoc.* **2008**, *3*, 1139–1152.
(33) Hilton, G. R.; Jackson, A. T.; Thalassinos, K.; Scrivens, J. H. *Anal. Chem.* **2008**, *80*, 9720–9725.
(34) Gies, A. P.; Kliman, M.; McLean, J. A.; Hercules, D. M. *Macromolecules* **2008**, *41*, 8299–9301.

(35) Giles, K.; Pringle, S. D.; Worthington, K. R.; Little, D.; Wildgoose, J. L.; Bateman, R. H. *Rapid Commun. Mass Spectrom.* **2004**, *18*, 2401–2414.
(36) Pringle, S. D.; Giles, K.; Wildgoose, J. L.; Williams, J. P.; Slade, S. E.; Thalassinos, K.; Bateman, R. H.; Bowers, M. T.; Scrivens, J. H. *Int. J. Mass Spectrom.* **2007**, *261*, 1–12.
(37) Shvartsburg, A. A.; Smith, R. D. *Anal. Chem.* **2008**, *80*, 9689–9699.
(38) Uetrecht, C.; Versluis, C.; Watts, N. R.; Wingfield, P. T.; Steven, A. C.; Heck, A. J. R. *Angew. Chem., Int. Ed.* **2008**, *47*, 6247–6251.
(39) Van Duijn, E.; Barendregt, A.; Synowsky, S.; Versluis, C.; Heck, A. J. R. *J. Am. Chem. Soc.* **2009**, *131*, 1452–1459.
(40) Faull, P. A.; Korkeila, K. E.; Kalapothakis, J. M.; Gray, A.; McCullough, B. J.; Barran, P. E. *Int. J. Mass Spectrom.* **2009**, *283*, 140–148.
(41) Scarff, C. A.; Patel, V. J.; Thalassinos, K.; Scrivens, J. H. *J. Am. Soc. Mass Spectrom.* **2009**, *20*, 625–631.
(42) Hopper, J. T. S.; Oldham, N. J. *J. Am. Soc. Mass Spectrom.* **2009**, *20*, 1851–1858.
(43) Joerger, A. C.; Rajagopalan, S.; Natan, E.; Veprintsev, D. B.; Robinson, C. V.; Fersht, A. R. *Proc. Natl. Acad. Sci. U.S.A.* **2009**, *106*, 17705–17710.
(44) Leary, J. A.; Schenauer, M. R.; Stefanescu, R.; Andaya, A.; Ruotolo, B. T.; Robinson, C. V.; Thalassinos, K.; Scrivens, J. H.; Sokabe, M.; Hershey, J. W. B. *J. Am. Soc. Mass Spectrom.* **2009**, *20*, 1699–1706.
(45) Pukala, T. L.; Ruotolo, B. T.; Zhou, M.; Politis, A.; Stefanescu, R.; Leary, J. A.; Robinson, C. V. *Structure* **2009**, *17*, 1235–1243.
(46) Schenauer, M. R.; Leary, J. A. *Int. J. Mass Spectrom.* **2009**, *287*, 70–76.
(47) Ridenour, W. B.; Kliman, M.; McLean, J. A.; Caprioli, R. M. *Anal. Chem.* **2010**, *82*, 1881–1889.
(48) Atmanene, C.; Chaix, D.; Bessin, Y.; Declerck, N.; Van Dorsselaer, A.; Sanglier-Cianferani, S. *Anal. Chem.* **2010**, *82*, 3597–3605.
(49) Hilton, G. R.; Thalassinos, K.; Grabenauer, M.; Sanghera, N.; Slade, S. E.; Wyttenbach, T.; Robinson, P. J.; Pinheiro, T. J. T.; Bowers, M. T.; Scrivens, J. H. *J. Am. Soc. Mass Spectrom.* **2010**, *21*, 845–854.
(50) Williams, J. P.; Phillips, H. I. A.; Campuzano, I.; Sadler, P. J. *J. Am. Soc. Mass Spectrom.* **2010**, *21*, 1097–1106.
(51) Chan, Y.-T.; Li, X.; Soler, M.; Wang, J.-L.; Wesdemiotis, C.; Newkome, G. R. *J. Am. Chem. Soc.* **2009**, *131*, 16395–16397.
(52) Ren, X.; Sun, B.; Tsai, C.-C.; Tu, Y.; Leng, S.; Li, K.; Kang, Z.; Van Horn, R. M.; Li, X.; Zhu, M.; Wesdemiotis, C.; Zhang, W.-B.; Cheng, S. Z. D. *J. Phys. Chem. B* **2010**, *114*, 4802–4810.
(53) Perera, S.; Li, X.; Soler, M.; Schultz, A.; Wesdemiotis, C.; Moorefield, C. N.; Newkome, G. R. *Angew. Chem., Int. Ed.* **2010**, *49*, 6539–6544.
(54) Brocker, E. R.; Anderson, S. E.; Northrop, B. H.; Stang, P. J.; Bowers, M. T. *J. Am. Chem. Soc.* **2010**, *132*, 13486–13494.
(55) Thalassinos, K.; Grabenauer, M.; Slade, S. E.; Hilton, G. R.; Bowers, M. T.; Scrivens, J. H. *Anal. Chem.* **2009**, *81*, 248–254.
(56) Smith, P. J.; Knapman, T. W.; Campuzzano, I.; Malham, R. W.; Berryman, J. T.; Radford, S. E.; Ashcroft, A. E. *Eur. J. Mass Spectrom.* **2009**, *15*, 113–130.
(57) Gidden, J.; Bowers, M. T.; Jackson, A. T.; Scrivens, J. H. *J. Am. Soc. Mass Spectrom.* **2002**, *13*, 499–505.
(58) Jackson, A. T.; Scrivens, J. H.; Williams, J. P.; Baker, E. S.; Gidden, J.; Bowers, M. T. *Int. J. Mass Spectrom.* **2004**, *238*, 287–297.